

Numerical simulation and transmission power analysis of tapered optical fiber sensors

I. NAVRUZ*, M. BILSEL, F. ARI

Department of Electrical and Electronics Engineering, Faculty of Engineering, Ankara University, Ankara, Turkey

In this paper, the geometrical design parameters of tapered optical fibers and their effects on sensing of refractive index are investigated. The transmission power of the sensor is simulated by using finite difference beam propagation method. The simulations are run by changing geometrical parameters which are length of transition region, length of waist region and waist diameter. The simulation results show that design parameters strongly affect the sensor performance including sensitivity and sensing range. Moreover, it is shown that the sensing range can be adjusted and also the sensor sensitivity can be enhanced using the optimized design parameters.

Received June 30, 2016; accepted August 9, 2017)

Keywords: Beam propagation method, Optical RI sensor, Tapered fiber

1. Introduction

Optical fibers are used in data transmission and various types of applications such as illumination in inaccessible places, fiber laser, fiber optical splitter or coupler, optical amplifier, fiber optical filter, and also optical sensor. In recent years an increasing interest has been observed in optical fiber sensors, since they offer some superior features when compared to traditional electrical sensors. Immunity from electromagnetic interference, remote sensing ability, light weight, usage in hazardous environments and high data carrying capacity are some of the advantages of these sensors. Moreover easy fabrication, low-cost and fast responsivity make them powerful sensors especially for biomedical and chemical sensing applications. These sensors are capable to sense strain/stress [1-3], temperature [4-5], pressure [6] and biological or chemical analytes [7-9].

A standard single-mode fiber can be transformed into a refractive index (RI) sensor by tapering a small part of it, thus the resultant sensor is known as biconical tapered fiber sensor. Biconical tapered fibers are produced by heating and stretching the fiber simultaneously, so that the diameter of cladding and core are reduced at same rate [10-13]. At the tapered region, core and cladding become indistinguishable. As a result, almost all of the light is guided by the cladding which results an increase in the evanescent field. A typical biconical tapered fiber is shown in Fig. 1. It includes three regions: regions with declining and ascending diameter at both ends and a region with constant diameter commonly known as waist in the middle. The uniform fiber region before descending region will be called as input fiber and the uniform fiber region following the ascending region will be called as output fiber. In this paper, heating and stretching processes are assumed to be done perfectly, so the lengths of both declining and ascending regions are equal and they are specified by L_1 in the figure. The length and diameter of

the waist region are shown by L_2 and R_w , respectively, in the figure.

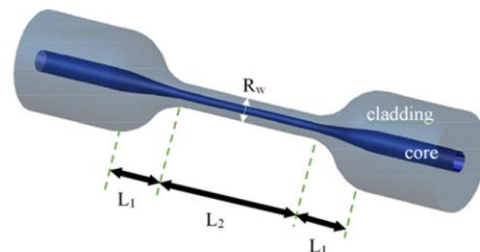


Fig. 1. A typical biconical tapered fiber sensor

When the wave propagates through the taper region indicated by L_1 length in Fig. 1, the fundamental mode will be degenerate, because the field distribution varies depending on the core and cladding diameters along the way. According to local tapering slope, the optical power in the fundamental mode is transferred to a few closest higher order modes. Fiber diameter decreases to waist diameter at the end of first tapered region so core is almost or wholly disappeared. As a result, the cladding acts as a new core and the medium surrounding the fiber is now the new cladding. When a change occurs in the refractive index of the medium, propagation constants of the modes will change due to the large difference of the RIs of cladding and medium. This will lead to optical power oscillations in the response of tapered fiber and it may also cause transmission loss at the end of the fiber output.

Tapered fibers can be classified as adiabatic and non-adiabatic according to tapering slope of both end regions with lengths L_1 as seen in Fig. 1. In the adiabatic structure, small relative change should be allowed in decreasing fiber radius at taper region. If the tapering slope from unaltered fiber to tapered fiber is very gradual, single-mode is only coupled into lowest order mode (HE_{11})

without coupling to higher order modes so most of optical power remains in this fundamental mode and loss of the light is negligible.

When the slope of ascending and descending regions at both ends of the tapered fiber is very steep, the structure is called nonadiabatic. In such a structure, fundamental mode is coupled into higher order modes, mostly into first two lower order modes HE_{11} and HE_{12} [14]. These modes propagate along the taper with different phases depending on taper length, RI of fiber and surrounding medium. All modes couple back to the fundamental mode after leaving waist region. As a result of coupling fundamental mode into higher order modes, the relative phase difference and output intensity are given as [15]

$$\Delta\phi_{mn} = \Delta\beta_{mn}l = \int_0^l [\beta_m(z) - \beta_n(z)] dz \quad (1)$$

$$I = \sum_{m=1}^N I_m + 2 \sum_{m>n} \sum_{n=1}^N \sqrt{I_m I_n} \cos\Delta\phi_{mn} \quad (2)$$

where l is length of the taper, N is the total number of modes supported by tapered fiber, I_m is the intensity of HE_{1m} mode and $\Delta\beta_{mn}$ is the difference of propagation constants of the modes. Changing either $\Delta\beta$ or l will cause a shift on power transmission versus wavelength or RI axes. Phase difference between propagation constants of any two modes is related to effective RI,

$$\Delta\beta = \frac{2\pi}{\lambda} \Delta n_{eff} \quad (3)$$

where λ is wavelength, Δn_{eff} is effective RI which depends on refractive index of fiber and the surrounding medium.

The finite difference beam propagation method (BPM) is a powerful technique to simulate lightwave propagation in tapered optical fibers like slowly varying optical waveguides. This method is based on slowly varying envelope approximation that solves Maxwell's equations with paraxial approximation by using finite differences in place of partial derivatives. More detailed information and numerical implementation about this method are given in [16-18], and a few commercially available software packages, for example by Optiwave and RP Photonics companies, can be found.

In this paper, the normalized transmission power of BTF sensor is simulated numerically using BPM. The transferred light powers related to RI are analyzed for different sensor designs by changing its geometrical design parameters, L_1 , L_2 and R_w . Finally, the effect of these parameters on the RI sensitivity and sensing range of the sensor are investigated.

The uniform fiber parameters are compatible with standard single mode fiber parameters of 9 μm core radius, 125 μm cladding radius, 1.45 and 1.445 core and cladding refractive indices, respectively. In all simulations

refractive index of the medium is varied between 1.30 and 1.40. The length of uniform fiber called as output fiber following the ascending region must be sufficiently long to ensure that light is coupled to single mode at the output of uniform fiber [19]. In our designs, the length of the output fiber is about 2 cm. The wavelength of light is 1.55 μm and mode calculation is evaluated for standard single mode fiber before launching the light into the input fiber.

2. Simulation results

In order to investigate the effect of design parameters on optical BTF sensor characteristics, firstly, the simulation was run for sensors having different waist diameters. The normalized power transmissions obtained for different waist diameter values are shown in Fig. 2. In these simulations, other geometrical parameters L_1 and L_2 are kept constant at 1200 and 1500 μm , respectively. When the waist diameter is increased, the transition geometry of tapered region becomes smooth in such a form that it can be called more adiabatic. On the other hand, reducing the waist diameter causes a steeper transition region so-called more nonadiabatic. Nonadiabaticity resulting from reduction of the waist diameter leads to high coupling ratio between unaltered fiber and tapered fiber that increases power oscillation at the output of the fiber as shown in Fig. 2. This result can be expected if it is considered that a smaller waist diameter stimulates the interaction of the guided field with the surrounding medium. In addition, smaller waist diameter decreases sensing range of the sensor. It is clearly seen from Fig. 2 that sensor with diameter of 20 μm has the longest RI sensing range. However, sensitivity decreases because of little power fluctuations which cannot be measured due to sensor's detection limit. By changing the waist diameter, a specific RI measurement range with acceptable power resolution can be adjusted.

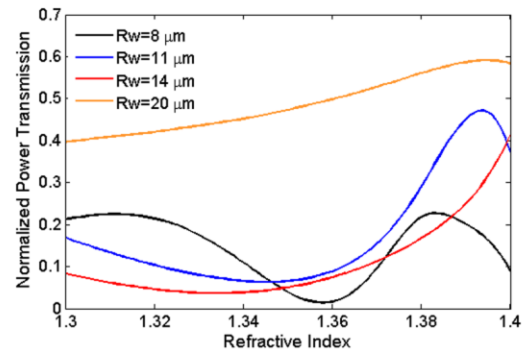


Fig. 2. Normalized power transmission of BTF sensors with different waist diameters, 8, 11, 14 and 20 μm

The sensitivity of the sensor can be defined as $\Delta P / \Delta n$ for approximately linear part of optical power fluctuation curve. R-squared value which is commonly used as an indicator of how well the linear curve fits the

data can test the linearity of sensor. The R-squared value reaches to 1 at maximum when the fitted line is exactly linear. In this paper, R-squared value for sensitivity analyses is calculated as 0.996 at minimum so that it can be considered as excellent. In this way, the sensitivity in normalized transmitted power per RI unit is calculated as 15.786 RIU^{-1} and 2.795 RIU^{-1} for two sensors with different waist diameters of 11 and 20 μm , respectively. Also, these sensors can measure refractive index between 1.371-1.391 and 1.340-1.394 intervals and the results are plotted in Fig. 3.

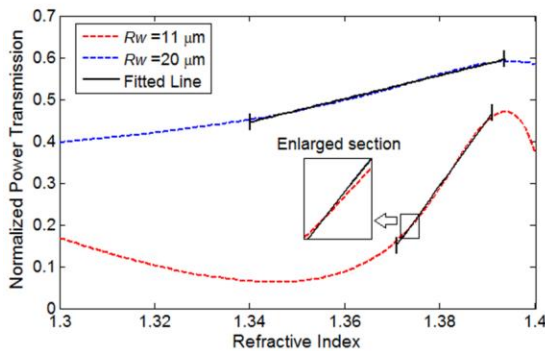


Fig. 3. Normalized power transmission and sensing range represented by fitted line for waist diameters $R_w=11$ and $20 \mu\text{m}$

In the second step of simulation studies, the influence of length L_1 on sensor characteristic has been investigated by keeping waist length L_2 constant at 1500 μm . The length of transition region L_1 is varied from 800 μm to 1300 μm with steps of 100 μm while waist diameter was 14 μm . The results are presented in Fig. 4(a-f).

The variation of L_1 parameter caused significant amount of variation in power oscillation curves. When Fig. 4 is examined in detail, it is seen that L_1 affects the position of the oscillation. However oscillation frequency is not affected. In other words, the power transmission graphics have one peak (negative or positive) in the RI range of 1.30-1.40. Simulation results obtained using smaller step size for L_1 are given in Fig. 5(a) and (b). In these simulations R_w and L_2 are kept constant at 14 μm and 1500 μm , respectively, and L_1 is changed between 930-970 μm for Fig. 5(a) and 1080-1120 μm for Fig. 5(b) with 5 μm steps.

As seen from both figures, when the parameter L_1 increases with 5 μm step size, power oscillation shifts towards right and a little change in its shape is observed as well.

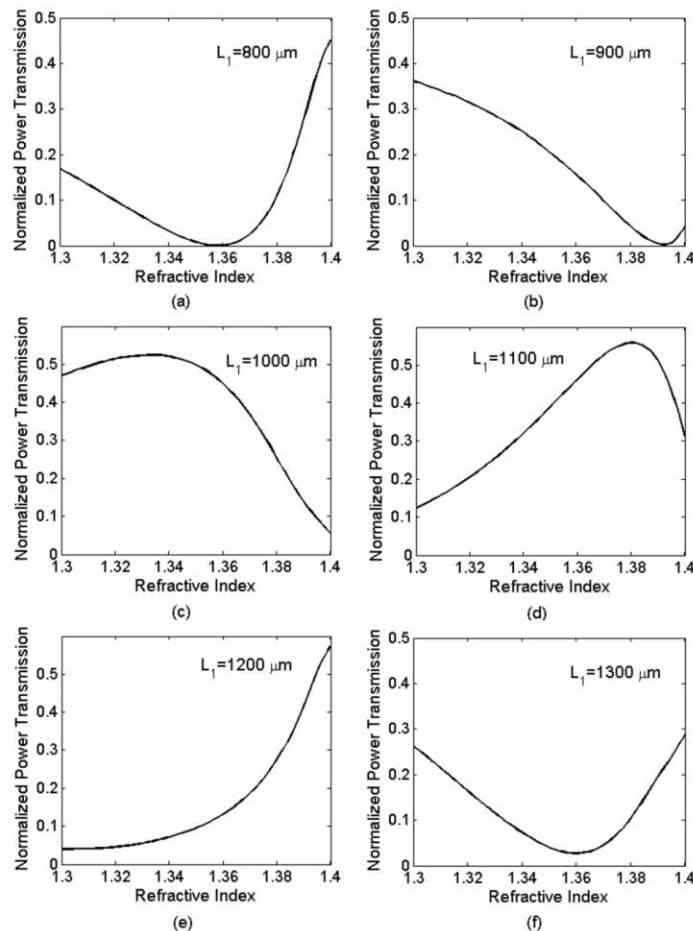


Fig. 4. Normalized power transmission for variation of L_1 between 800-1300 μm , $R_w=14 \mu\text{m}$, $L_2=1500 \mu\text{m}$

This shift caused by variation of L_1 was observed in all the simulations for different sensor designs. Both the shifting effect and the little change in oscillation shape will change the sensitivity of the sensor and sensing range of the sensor will also be affected. For example, if it is desired to measure RI between 1.36 and 1.40, the sensor design with $L_1 = 970 \mu\text{m}$ in Fig. 5(a) can be chosen as the most suitable. On the other hand, the power variation versus RI for the sensor design with $L_1 = 1080 \mu\text{m}$ in Fig 5(b) is almost linear between 1.30 and 1.36. Thereby this is the most suitable design to make measurement in that interval.

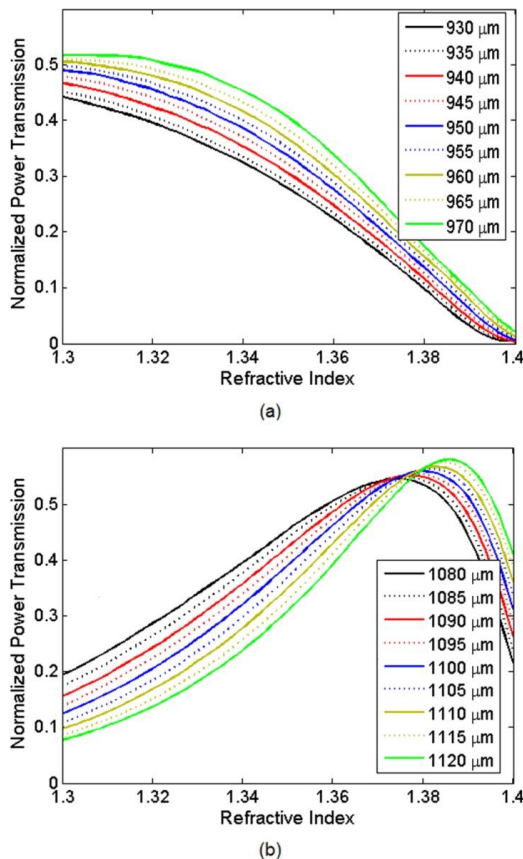


Fig. 5. The simulation results for variation of L_1 by step size of $5 \mu\text{m}$ between (a) $930\text{-}970 \mu\text{m}$, (b) $1080\text{-}1120 \mu\text{m}$, when $R_w = 14 \mu\text{m}$, $L_2 = 1500 \mu\text{m}$.

When L_1 is increased to a few thousand micrometers, transition from untapered fiber to tapered fiber becomes very gradual. In this study, L_1 is increased to nearly $5000 \mu\text{m}$ to analyze its effect on power transmission when R_w and L_2 were kept constant at 14 and $1500 \mu\text{m}$, respectively. Fig. 6 demonstrates power transmission of sensors with different values of L_1 between $1600\text{-}5350 \mu\text{m}$ and sensing ranges with fitted R-squared value. The minimum calculated R-squared value is 0.996 . Some specific values for L_1 were chosen among lots of simulations to compare the power transmission of sensors whose characteristics are similar. Using the curves in Fig 5, RI sensing ranges of the sensors are calculated as 0.057 , 0.044 , 0.040 and 0.035 for L_1 equal to 1600 , 3450 and $5350 \mu\text{m}$, respectively. It is clearly noted that as L_1 increases RI sensing range becomes narrow but sensor

sensitivity does not exhibit a significant amount of difference.

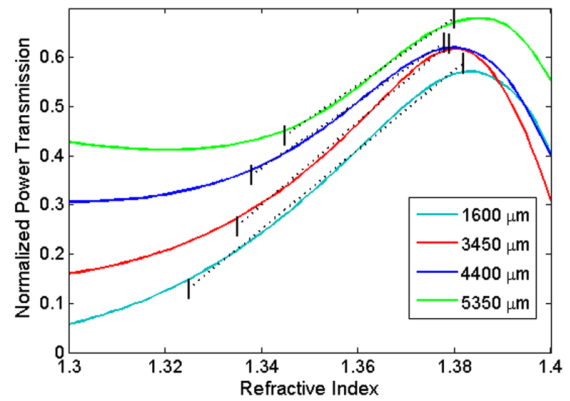


Fig. 6. Normalized power transmissions for longer L_1 values

Another geometrical parameter that can affect characteristics of biconical tapered fiber sensors is the length of waist region that is symbolized as L_2 . The simulation results obtained for different values of L_2 are shown in Fig. 7. The parameter L_2 is increased with $50 \mu\text{m}$ step size between $1000\text{-}1400 \mu\text{m}$ and $5 \mu\text{m}$ step size between $1430\text{-}1470 \mu\text{m}$ in Fig. 7 (a) and (b), respectively. Here R_w and L_1 parameters are kept constant at 14 and $1000 \mu\text{m}$, respectively.

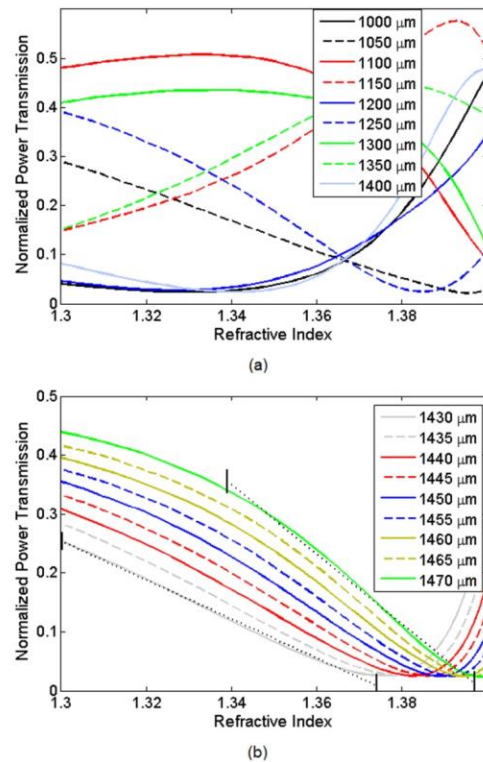


Fig. 7. The simulation results obtained for different length of waist region, L_2 that increased by step size of (a) $50 \mu\text{m}$ between $1000\text{-}1400 \mu\text{m}$ and (b) $5 \mu\text{m}$ between $1400\text{-}1470 \mu\text{m}$, other parameters are $R_w = 14 \mu\text{m}$, $L_1 = 1000 \mu\text{m}$

As seen from Fig. 7(a), the normalized power transmission curves exhibit different oscillations those have single positive or negative peak point in the RI range of 1.30-1.40 for different values of L_2 . Increasing L_2 causes the power oscillations to shift like the effect of L_1 . Therefore, the sensing range and the sensor sensitivity can also be controlled with L_2 . The normalized power transmission curves for L_2 between 1430 and 1470 μm are given in Fig. 7(b). It is seen that the sensor designed for $L_2=1430$ μm can operate in range of 1.300-1.374 with the calculated sensitivity of 3.3128 RIU^{-1} . On the other hand, the sensor with $L_2=1470$ μm can operate in range of 1.339-1.397 with sensitivity of 5.9038 RIU^{-1} .

In order to analyze the sensor characteristics of biconical tapered fiber having longer waist region, the value of L_2 has been increased from 1800 to 1950 μm in Fig. 8(a) and from 5100 to 5250 μm in Fig. 8(b) with 50 μm step size without changing R_w and L_1 parameters. It is clearly seen that as L_2 increases the frequency of oscillation also increases. The reason for the increase in fluctuation frequency is that the longer waist region allows the optical power to be transferred to higher order modes, thus, higher slope changes occur in the power oscillations. This response of the sensor can be used to perform more sensitive measurement in a special range of RI.

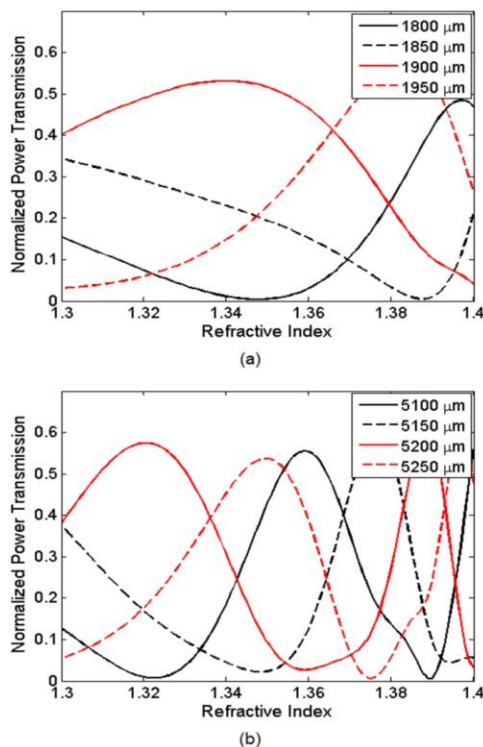


Fig. 8. Normalized power transmissions for longer L_2 increased by step size of 50 μm between (a) 1800-1950 μm (b) 5100-5250 μm

The response of the sensor by changing L_2 with 800 μm steps is illustrated in Fig. 9. It is noted that oscillation curves in Fig. 9(a) for different L_2 values are similar to each other. Here the curves have negative peaks around 1.38 RI. When the initial value of L_2 is chosen as 1950 μm

and increased with 800 μm steps without changing other design parameters, the obtained power oscillation curves are again similar to each other as seen in Fig. 9(b). Here the curves have positive peaks around RI of 1.38. The power oscillation curves in Fig. 9(a) show negative trends within RI range of about 1.34-1.38, while the curves in Fig. 9(b) show positive trends approximately the same range of RI. As it is seen from Fig. 8 and Fig. 9, many sensor responses including desired RI sensing range and sensitivity can be obtained by controlling the parameter L_2 .

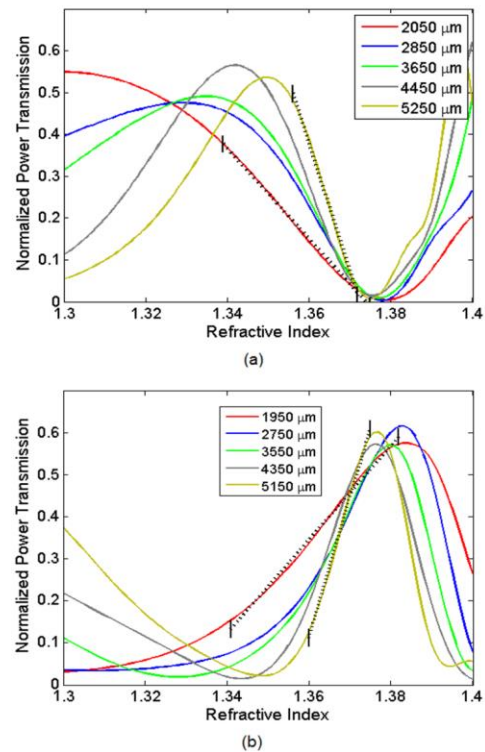


Fig. 9. Normalized power transmission curves whose characteristics are similar to each other when L_2 is changed with 800 μm step size. The initial value of L_2 is chosen as (a) 2050, and (b) 1950 μm

When L_2 is increased by 800 μm step size, it is obtained that the sensor sensitivity is improved. However, the value of 800 μm step size is specific to this sensor design and it may be altered for different sensor designs in order to compare analogous power oscillation curves. The fitted lines are shown as black dotted lines in Fig. 9 and the sensitivities are calculated as 10.36 and 30.18 RIU^{-1} for the sensors with L_2 values of 2050 and 5250 μm , respectively.

The sensitivity and sensing range variation versus length L_2 calculated from Fig. 9(a) and (b) are shown in the first and last three columns of Tab. 1, respectively. As seen in the table, the sensitivity variation with L_2 is not linear. However, it is clear that the sensitivity increases as L_2 increases. On the other hand, the sensing range decreases while sensitivity increases.

Table 1. Sensitivity and sensing range variation versus waist length

Negative Slope Section		
L_2 (μm)	Sensitivity (RIU^{-1})	Sensing Range (RI)
2050	10.36	0.048
2850	15.17	0.028
3650	17.06	0.026
4450	23.57	0.022
5250	30.18	0.016
Positive Slope Section		
L_2 (μm)	Sensitivity (RIU^{-1})	Sensing Range (RI)
1950	11.15	0.041
2750	18.72	0.024
3550	19.39	0.022
4350	26.13	0.019
5150	33.15	0.015

3. Conclusion

In this study, the optical power response of biconical tapered fiber as a refractive index sensor is numerically simulated for various waist radius, length of transition region and length of waist region values symbolized as R_w , L_1 and L_2 , respectively. These geometrical design parameters of BTF sensors strongly affect their RI sensing characteristics especially sensor sensitivity and sensing range. When R_w is increased gradually from 8 to 20 μm , the sensing range increases, but sensitivity decreases. Variation of L_1 leads to significant changes in the power oscillations; however, the oscillation frequency is not affected. If L_1 is increased a few μm , the transmission power oscillation versus RI slightly shifts towards to right. When L_1 is increased to a few thousand μm , the sensing range decreases but sensitivity doesn't increase. On the other hand, if L_2 is increased a few μm , the transmission power oscillation versus RI slightly shifts towards to right similar to effect of L_1 . When L_2 is increased to a few thousand μm , the sensitivity increases in a slightly narrower sensing range as a result of higher change in the power oscillation due to excitation of higher order modes. This response of the sensor can be used to perform more sensitive measurement in a particular range of RI.

Acknowledgements

This work was supported by the Scientific and Technological Research Council of Turkey (TUBITAK) under Project: 114E040.

References

- [1] S. W. Choi, J. Lee, B. H. Oh, H. S. Park, International Journal of Distributed Sensor Networks, Article ID: 894780, 9 pages (2013).
- [2] E. Li, IEEE Photonics Technology Letters **19**, 1266 (2007).
- [3] C. R. Dennison, P. M. Wild, D. R. Wilson, M. K. Gilbert, Measurement Science and Technology **21**, 115803 (2010).
- [4] S. Zhu, J. W. Xing, F. F. Pang, T. Y. Wang, Journal of Shanghai University **15**, 101 (2011).
- [5] M. K. Saxena, S. D. V. J. Raju, R. Arya, R. B. Pachori, S. V. G. Ravindranath, S. Kher, S. M. Oak, Optics & Laser Technology **65**, 14 (2015).
- [6] N. Wu, Y. Tian, X. Zou, Y. Zhai, K. Barringhaus, X. Wang, Sensors and Actuators B: Chemical **181**, 172 (2013).
- [7] Q. Meng, X. Dong, K. Li, Y. Ni, B. Xu, Z. Chen, IEEE Sensors Journal **14**, 1813 (2014).
- [8] S-H. Ohk, A. K. Bhunia, Food Microbiology **33**, 164 (2013).
- [9] M. I. Zibaii, H. Latifi, Z. Saeedian, Z. Chenari, Journal of Photochemistry and Photobiology B: Biology **134**, 55 (2014).
- [10] S. W. Harun, K. S. Lim, C. K. Tio, K. Dimiyati, H. Ahmad, Optik - International Journal for Light and Electron Optics **124**, 538 (2013).
- [11] A. Leung, K. Rijal, P. M. Shankar, R. Mutharasan, Biosensors and Bioelectronics **21**, 2202 (2006).
- [12] S. Pricking, H. Giessen, Optics Express **18**, 3426 (2010).
- [13] H. Latifi, M. I. Zibaii, S. M. Hosseini, P. Jorge, Photonic Sensors **2**, 344 (2012).
- [14] G. Cohoon, C. Boyter, M. Errico, K. Vandervoort, E. Salik, Optical Engineering **49**, 034401 (2010).
- [15] Y. Tan, J. Lou, H. Xu, J. Huang, W. Shen, International Symposium on Photoelectronic Detection and Imaging, Proc. of SPIE **8914**, 891407 (2013).
- [16] Y. Chung, N. Dagli, IEEE Journal of Quantum Electronics **26**, 1335 (1990).
- [17] S. A. Shakir, R. A. Motes, R. W. Berdine, IEEE Journal of Quantum Electronics **47**, 486 (2011).
- [19] M. S. Wartak, Computational Photonics, an Introduction with MATLAB. Cambridge University, 2013.
- [20] W. Klaus, W. R. Leeb, Optics Express **15**, 11808 (2007).

*Corresponding author: inavruz@ankara.edu.tr